Letters

Simplified Integration of Bidirectional OBC and WPT Charging Systems With Reconfiguring Topology for Electric Vehicles

Cheol-Hee Jo, *Member, IEEE*, and Dong-Hee Kim, *Member, IEEE*

***Abstract*—This letter proposes a simplified integration system of bidirectional on-board chargers (OBC) and wireless power transfer (WPT) charging systems for electric vehicles. The proposed system reduces the cost, weight, and volume of the power conversion units by sharing active switch bridges and magnetic coupler coils without mechanical switches. The proposed magnetic coupler design method enables the secondary coil to be shared in both OBC and WPT modes, while the primary coil for OBC can be magnetically decoupled from the transmitter coil in WPT mode. Based on the proposed topology configuration and winding method, the proposed system operates as a dual-active bridge and an inductor-capacitor-capacitor-series (LCC-S) compensated converter in the OBC and WPT modes, respectively. To validate the proposed integrated OBC and WPT charging system, a prototype with a 3.3-kW OBC and WPT system is configured and verified through experiments.**

***Index Terms*—Bidirectional, electric vehicles (EVs), on-board charger (OBC), wireless power transfer (WPT).**

I. Introduction

ELECTRIC vehicles (EVs) have gained significant attention worldwide due to concerns about greenhouse gas emissions, leading to research on charging technologies for high efficiency, safety, and convenience [1]. Generally, charging technologies for EVs can be divided into wired and wireless charging. The wired charging system is classified into on-board chargers (OBCs) and off-board chargers. The wireless charging system consists of a transmitting system that transmits power from the utility and a receiving system that receives power to vehicles. The OBC and receiver system, mounted in the limited space of the vehicle, require high power density. However, EVs equipped with both OBC and wireless power transfer (WPT) charging systems end up with two separate charging systems, increasing the weight, cost, volume, and complexity.

To overcome these limitations, many studies [2], [3], [4], [5], [6], [7], [8], [9] on the integration of wired and wireless charging systems are increasing due to the similar power conversion stages between wired and wireless charging systems. Wu et al. [2] proposed the integrated charging system of an off-board charger and WPT charging system. Even though the integrated system improves the power density by reusing the inverter and the resonant network on the transmitter side, the OBC and receiver system inside the vehicles are still required for wired and wireless charging. In [3], the rectifier on the receiver side in the vehicles is shared for both wired and wireless charging systems. The integrated OBC and WPT charging system [4] improves the power density by sharing not only the rectifier but also the resonant capacitors on the receiver side through the added receiver coil for the WPT charging system. In [5] and [6], the inductor is integrated with the magnetic coupler coils to reduce the cost and volume of the system. In [7], a magnetic coupler design method was proposed for the integration of the OBC and WPT charging systems. Similarly, the authors in [8] and [9] proposed an integrated WPT and auxiliary power module for EVs that share switches and magnetic coupler coils. However, the above conventional integrated systems [3], [4], [5], [6] have limitations in increasing power density because they do not integrate magnetic coupler coils for OBC and WPT charging systems. Although the integrated charging systems [7], [8], [9] improve the power density by sharing the switch bridge and magnetic coils for wired and wireless charging, they require mechanical switches [7], [8], and the frequency bifurcation or frequency splitting issue can be observed according to load and coupling coefficient conditions [9]. In addition, since these integrated charging systems [7], [8], [9] have only been validated under aligned conditions in the WPT mode, the feasibility of their operation under misaligned conditions in the WPT mode remains unclear.

This letter proposes a simplified integration system of bidirectional OBC and WPT charging systems that shares the switch bridges and magnetic coupler coils. The proposed magnetic coupler design method enables the secondary coil to be shared in both OBC and WPT modes, while the primary coil for OBC is magnetically decoupled from the transmitter coil for WPT in WPT mode without mechanical switches. Based on the proposed topology configuration and magnetic coupler design method, the proposed system operates as a conventional dual-active bridge (DAB) and LCC-S compensated converters in the OBC and WPT modes, respectively. To validate the proposed integrated OBC and WPT charging system, a prototype featuring a 3.3-kW

Received 12 December 2024; revised 21 January 2025; accepted 6 February 2025. Date of publication 10 February 2025; date of current version 20 March 2025. This work was supported by Korea Electric Power Corporation under Grant R23X007-05. *(Corresponding author: Dong-Hee Kim.)*

The authors are with the Chonnam National University, Gwangju 61186, South Korea (e-mail: 218249@jnu.ac.kr; kimdonghee@jnu.ac.kr).

Color versions of one or more figures in this article are available at https://doi.org/10.1109/TPEL.2025.3540516.

Digital Object Identifier 10.1109/TPEL.2025.3540516

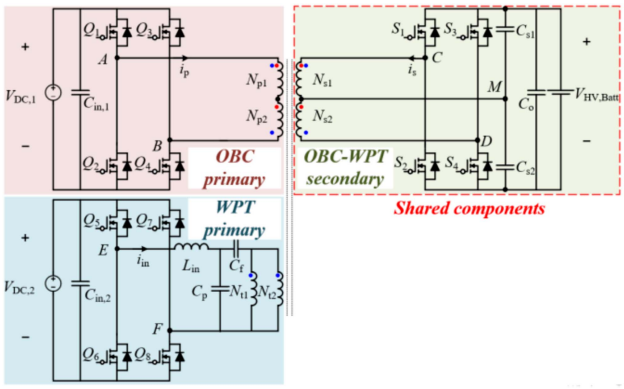

Fig. 1. Proposed integrated OBC and WPT charging system.

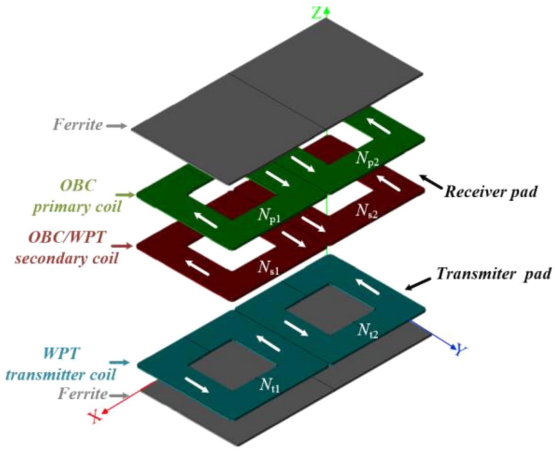

Fig. 2. Pad structure of proposed charging system.

OBC and WPT system is developed and experimentally verified under charging and discharging conditions in OBC mode, as well as under aligned and misaligned conditions in WPT mode.

II. Operating Principle of the Proposed Integrated Charging System

A. Topology Description of the Proposed Charging System

Fig. 1 shows the proposed integration charging system of OBC and WPT. This system has two operation modes: bidirectional OBC and WPT modes, and comprises three H-bridges: the OBC primary, WPT primary, and OBC/WPT secondary bridges. A compensation network consisting of a compensation inductor and capacitors (L_{in}, C_{f}, and C_{p}) is configured on the WPT primary side. On the OBC/WPT secondary side, the compensated capacitors (C_{s1} and C_{s2}) are placed. The H-bridge of the OBC/WPT secondary is shared for OBC and WPT modes. A power factor correction converter is connected upstream of the OBC primary; however, this article focuses on the dc–dc converter of the OBC.

As shown in Fig. 2, the receiver pad consists of ferrite and multilayer coils and each layer consists of OBC primary and OBC/WPT secondary coils. The OBC primary (OBC/WPT secondary) winding is separated into oppositely wound coils,

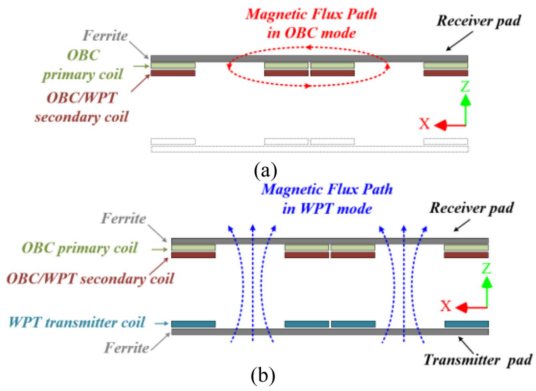

Fig. 3. Schematic of magnetic flux path in (a) OBC and (b) WPT modes.

N_{p1} and N_{p2} (N_{s1} and N_{s2}), which are connected in series, as shown in Fig. 2. Therefore, in OBC mode, the magnetic flux path is configured, as shown in Fig. 3(a). On the other hand, on the transmitter pad for WPT mode, the WPT transmitter windings consist of two rectangular coils (N_{t1} and N_{t2}) with the same winding directions. In WPT mode, under this coil structure, the magnetic flux path generated by the WPT transmitter coil is shown in Fig. 3(b). Here, since N_{p1} and N_{p2} (N_{s1} and N_{s2}) of the OBC primary (OBC/WPT secondary) winding are wound oppositely, each voltage induced in N_{p1} and N_{p2} (N_{s1} and N_{s2}) has opposite polarities. As shown in Fig. 1, the polarity of each coil is indicated in red and blue dots for the OBC and WPT modes, respectively. The voltages induced in N_{p1} and N_{p2} (N_{s1} and N_{s2}) cancel each other out due to their opposite polarities, resulting in no voltage being induced in the OBC primary (OBC/WPT secondary) winding. However, in contrast to the OBC primary side, the connection point M of N_{s1} and N_{s2} on the OBC/WPT secondary side is connected to the compensated capacitors (C_{s1} and C_{s2}) to form a path through which voltage by the WPT transmitter coils can be induced, as shown in Fig. 1. In other words, the OBC/WPT secondary coil can be reconfigured according to the OBC and WPT modes. Therefore, the WPT transmitter coils are coupled with only the OBC/WPT secondary coils, not the OBC primary coils. Consequently, the OBC/WPT secondary coils can be shared for OBC and WPT modes.

B. Operating Principle of the Proposed Charging System

Based on the described topology configuration and winding method, the circuit configuration and coil polarity can be reconfigured for both OBC and WPT modes. As shown in Fig. 4(a), in OBC mode, the operational topology of the proposed charging system is identical to the conventional DAB converter that transfers power using a linked inductor. In the proposed charging system, the leakage inductor $L_{\text{leakage,obc}}$ between the OBC primary and OBC/WPT secondary coils on the receiver pad is utilized as the linked inductor. In addition, C_{s1} and C_{s2} can be neglected due to the symmetry condition of the magnetic coupler coil, which is explained later. Thus, the proposed charging system operates as the bidirectional DAB converter, and the

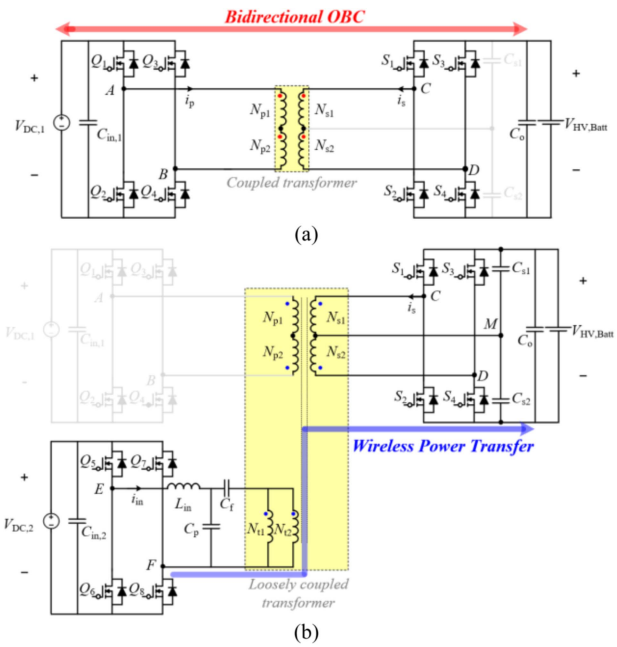

Fig. 4. Operating topology in (a) OBC and (b) WPT modes.

output voltage $V_{\mathrm{HV,Batt}}$ can be regulated by phase D between OBC primary and OBC/WPT secondary bridges are given as follows:

$$V_{\mathrm{HV,Batt}} = \frac{R_{\mathrm{HV,Batt}} V_{\mathrm{DC},1}}{2 n_1 f_{\mathrm{obc}} L_{\mathrm{leakage,obc}}} D\,(1-D) \tag{1}$$

where $R_{\mathrm{HV,Batt}}$, n_1, f_{obc}, and $V_{\mathrm{DC},1}$ are the dc output load and the turn ratio of the OBC primary, OBC/WPT secondary windings, switching frequency, and input voltage of OBC, respectively. Furthermore, other phase controls, such as dual phase shift as well as single phase shift control, can be implemented in the proposed charging system.

As shown in Fig. 4(b), in WPT mode, the operational topology of the proposed charging system is identical to the conventional LCC-S compensated converter that has load-independent output voltage characteristics [10]. However, since C_{s1} and C_{s2} on the OBC/WPT secondary side operate as voltage doublers as well as compensation capacitors, the LCC-S compensation parameters should be designed taking this into these characteristics. In addition, in WPT mode, the currents flowing through N_{s1} and N_{s2} are in phase. Consequently, C_{s1} and C_{s2} resonate with the inductance L_{s1} of N_{s1} and the inductance L_{s2} of N_{s2}, respectively, as given in (2). The reason why C_{s1} and C_{s2} are equal is due to the symmetry condition of the magnetic coupler coil ($L_{s1} = L_{s2}$), which is explained later

$$C_{s1} = C_{s2} = \frac{1}{\omega_r^2} L_{s1} = \frac{1}{\omega_r^2 L_{s2}}. \tag{2}$$

The WPT transmitter coils (N_{t1} and N_{t2}) are configured in parallel, as shown in Fig. 4(b), but even if they are configured in series, the magnitude of the voltage and current stress applied to the coils (N_{t1} and N_{t2}) is the same. The remaining parts can be designed considering the zero-phase angle and output voltage characteristics, the same as the conventional LCC-S compensated converter [10]. The compensated parameter design method is omitted due to the limited space in this article [10]. Based on the above explanation, in WPT mode, the proposed charging system operates as the conventional LCC-S compensated converter, and the output voltage $V_{\mathrm{HV,Batt}}$ can be regulated by switching frequency control or phase shift control [11], [12].

To ensure the normal operation of the proposed charging system in both OBC and WPT modes, a symmetrical design of the proposed magnetic coupler coils is required.

First, a symmetrical design of the N_{p1} and N_{p2} (N_{s1} and N_{s2}) coils is necessary to prevent circulating current through C_{s1} and C_{s2} in the OBC mode. In addition, a symmetrical design of the N_{t1} and N_{t2} coils is essential to ensure equal power sharing between the N_{s1} and N_{s2} coils and to guarantee decoupling from the OBC primary side in the WPT mode.

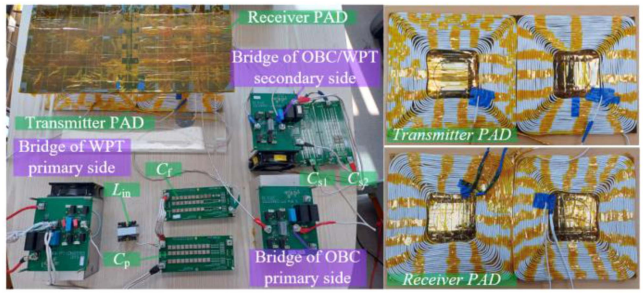

Fig. 5. Photography of experimental prototype.

TABLE I
SPECIFICATIONS OF THE PROPOSED CHARGING SYSTEM

Parameters	Values
V_{DC1} and V_{DC2}	365 V
$V_{\mathrm{HV,Batt}}$ and $P_{\mathrm{out,rated}}$	400 V and 3.3 kW
f_{obc} and f_{wpt}	102 kHz and 81–85 kHz
N_{p1}: N_{s1}: N_{t1}	23 : 23 : 23
L_{p}, L_{s}, and L_{t} in WPT mode	50.8 μH, 103.3 μH, and 113.5 μH
k_{ps} in OBC mode	0.944
k_{ps}, k_{pt}, and k_{st} in WPT mode	0.008, 0.010, and 0.147
L_{in}, C_{f}, C_{p}, C_{s1}, and C_{s2}	29.6 μH, 41.6 nF, 119.9 nF, 16.9 nF, and 16.8 nF
Tx and Rx pad dimensions	295 mm × 590 mm
Air gap and misalignment	125 mm (Z-axis) and ±30 mm (X-and Y-axes)

III. EXPERIMENTAL RESULTS

To verify the effectiveness of the proposed charging system, a 3.3-kW OBC and WPT experimental prototype has been build, as shown in Fig. 5. The specifications of the proposed system are listed in Table I, where L_{p}, L_{s}, and L_{t} are the measured self-inductance of each coil in WPT mode. In Table I, the coupling coefficient (k_{ps}, k_{pt}, and k_{st}) between each coil in OBC and WPT modes is derived from the measured values by the *LCR* meter. Please note that L_{s} is measured in OBC and WPT modes with the separated N_{s1} and N_{s2} connected in series and parallel. With the measured coupling coefficients, as shown in Table I, the OBC primary coil and the OBC/WPT secondary coil are strongly coupled in OBC mode, and in WPT mode, the WPT transmitter coils are coupled with only

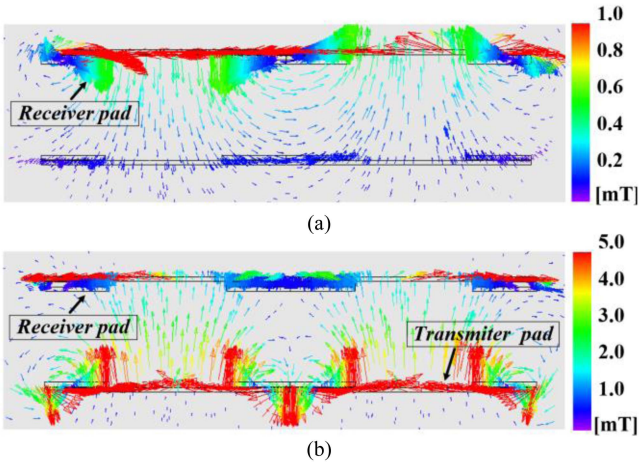

Fig. 6. Magnetic flux density vector plot of magnetic pads in (a) OBC and (b) WPT mode by JMAG simulation.

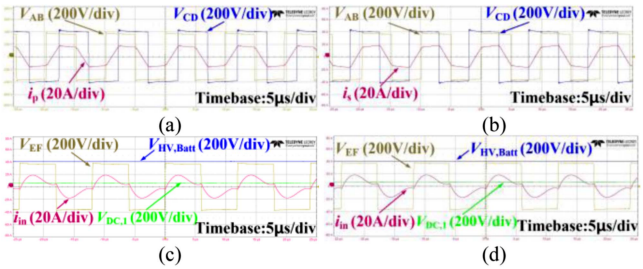

Fig. 7. Experimental waveforms of the proposed system at 3.3-kW output power in (a) OBC charging, (b) OBC discharging, (c) WPT alignment, and (d) WPT misalignment.

the OBC/WPT secondary coils, not the OBC primary coils. Fig. 6 shows the magnetic flux density vector plot by JMAG finite element analysis simulation in OBC and WPT modes. Based on the JMAG simulation, the maximum magnetic flux density is 122.2 and 60.2 mT in the OBC and WPT modes, respectively.

Fig. 7 shows the experimental waveforms at the rated output power $P_{\mathrm{out,rated}}$ of 3.3-kW in charging and discharging modes of OBC, and alignment and misalignment conditions of WPT mode. It can be seen that the proposed charging system operates as the DAB converter and LCC-S compensated converter in OBC and WPT modes, respectively. To regulate the output voltage to 400 V, the proposed system uses single phase and frequency control in OBC and WPT modes, respectively. In WPT mode, although the dc-link voltage on the OBC primary side can occur from 52 to 150 V depending on the severity of the misalignment condition, as shown in Fig. 7, this magnitude can be acceptable as 41.1% of the input voltage 365 V. This occurs because greater X-axis misalignment leads to more voltage differences between N_{p1} and N_{p2}. Fig. 8 shows the measured efficiency of the proposed charging system in OBC and WPT modes. Overall, it has higher efficiency in OBC mode than WPT mode, with maximum efficiencies of 97.59% and 94.14% in OBC and WPT modes, respectively. In contrast to OBC mode, WPT mode has losses of the WPT primary side components that remain nearly constant

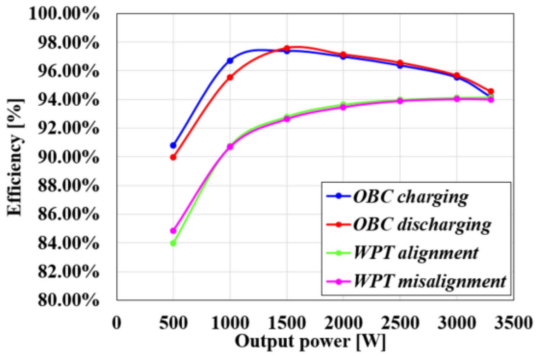

Fig. 8. Measured efficiency of the proposed system in OBC and WPT modes.

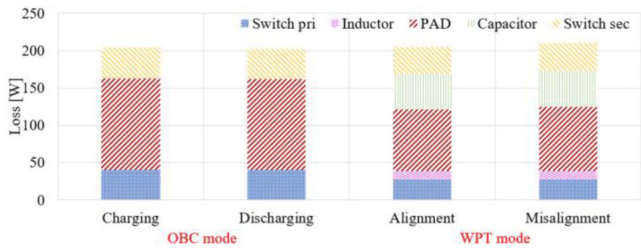

Fig. 9. Loss breakdown of the proposed charging system for each mode at a rated output power of 3.3 kW.

regardless of the load, which is also characteristic of the LCC-S compensation topology [10]. For this reason, WPT mode has lower efficiency than OBC mode across the overall load range, as shown in Fig. 8. In addition, the reason why there is no significant difference in efficiency under alignment and misalignment conditions in WPT mode is that the compensation parameters are designed based on the misalignment condition, so the switching frequency operates far from the resonant frequency under the alignment condition. This increases the circulating current and hard turn-OFF losses of the inverter, which is particularly critical under light load conditions, leading to lower efficiency under alignment compared with misalignment, as shown in Fig. 8 [12]. However, this may vary depending on the configuration and specifications of the WPT system. In other words, the difference in efficiency under alignment and misalignment conditions may exhibit different results depending on the control method and system specifications.

Based on loss calculations, JMAG simulation, and experimental results, Fig. 9 shows the loss breakdown of the proposed charging system at the rated output power of 3.3 kW. In OBC mode, the system losses can be divided into the OBC primary inverter, magnetic coupler pad, and OBC/WPT secondary inverter. In WPT mode, the losses are distributed across the WPT primary inverter, resonant inductor, resonant capacitors, magnetic coupler pad, and OBC/WPT secondary inverter. The proposed system operates near a zero-phase angle at rated power in WPT mode compared with OBC mode, resulting in a smaller circulating current and reduced losses in the primary inverter, as shown in Fig. 9. The larger loss of the magnetic coupler pad in OBC mode compared with WPT mode is due to the OBC/WPT

TABLE II
COMPARATIVE ANALYSIS WITH CONVENTIONAL INTEGRATED SYSTEMS

Parameters	Separated (OBC and WPT)	[2]	[4]	[7]	[8]	[9]	This work
Integration method	-	Off-board charger + WPT	OBC + WPT	OBC + WPT	APM + WPT	APM + WPT	OBC + WPT
Number of switches	12	8	12	12	12	12	12
Number of diodes	4	4	-	-	-	-	-
Number of transformers	1	1	1	-	1	-	-
Number of inductors	2	-	3	-	-	-	1
Number of relays	-	-	-	1	1	-	-
Power rating	3.3 kW	1 kW	7.7 kW	1.2 kW	1.2 kW	1.2 kW	3.3 kW

secondary side operating as a voltage doubler in WPT mode, which reduces the current.

IV. COMPARATIVE ANALYSIS

This section describes the features of the proposed integrated charging system compared with the existing charging systems [2], [4], [7], [8], [9]. First, in contrast to [2], the proposed charging system integrates bidirectional OBC and WPT receiver components within the limited space in EVs. Second, in comparison to [2], [4], and [8], the additional transformer is incorporated into the WPT receiver magnetic pad, leading to reductions in both cost and volume. Third, contrary to [9], the proposed integrated system operates in WPT mode as a conventional LCC-S compensation topology, which minimizes the possibility of bifurcation [13], [14], [15]. Fourth, in contrast to [7] and [8], the proposed system eliminates the need for additional mechanical switches, such as relays. Finally, as compared with [2], [7], [8], and [9], the proposed system has been experimentally validated under both aligned and misaligned conditions in WPT mode. Table II presents a comparison of the separated OBC and WPT charging systems, conventional integrated charging systems, and the proposed integrated charging system. In the separated OBC and WPT charging systems, the OBC is a DAB converter, while the WPT charging system consists of an LCC-S compensation topology, similar to the proposed system.

To compare the volume and cost of power conversion units, it makes sense to evaluate systems with equivalent functionality. However, the integration targets differ among the systems, as shown in Table II. For instance, the off-board charging system integrated in [2] requires only one H-bridge as a unidirectional power converter. In contrast, the OBC integrated into the proposed system requires at least two H-bridges as a bidirectional power converter. Therefore, the proposed system can be compared with [4] and [7] in terms of volume and cost, as they have the same integration targets. Since power ratings, magnetic components, and operating switching frequency ranges differ among systems, the following assumptions are necessary to compare the volume and cost of power conversion systems. First, the rated power of the system and the components and magnetic pads used are based on the specifications of the proposed system. Second, components not utilized in the proposed system are selected based on a rated power of 3.3 kW (e.g., PQ5050 for the transformer). Based on Table II and the above assumptions, Figs. 10 and 11 show the volume, power density, and cost of [4] and [7] and the proposed system. As shown in Figs. 10 and 11, the proposed system reduces volume by 10.88% and cost by 10.21% compared with the separated OBC and WPT systems. Although the results are based on certain assumptions and may lack complete accuracy, they provide a clear indication of the potential advantages of the proposed system.

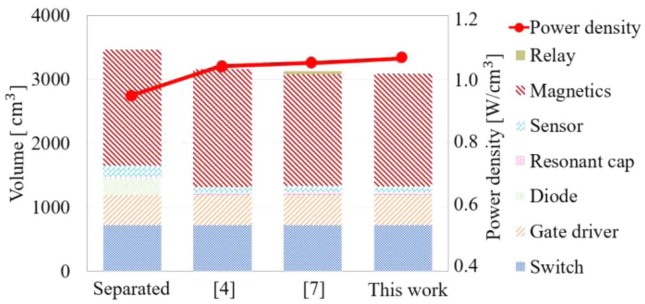

Fig. 10. Volume and power density of separated OBC and WPT chargers, conventional integrated OBC and WPT chargers, and the proposed integrated charger.

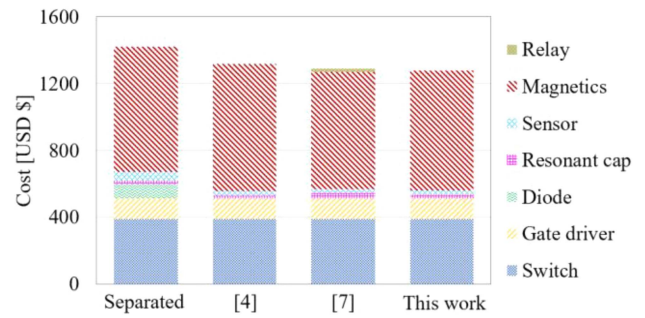

Fig. 11. Cost of separated OBC and WPT chargers, conventional integrated OBC and WPT chargers, and the proposed integrated charger.

V. Conclusion

This letter proposed a simplified integration system of bidirectional OBC and WPT charging systems that shares the switch bridges and magnetic coupler coils. It was verified that the proposed magnetic coupler enables the OBC/WPT secondary coil to be shared in both OBC and WPT modes, while the OBC primary coil is magnetically decoupled from the WPT transmitter coil in WPT mode without mechanical switches. The performance of the proposed charging system was evaluated under the charging and discharging conditions of OBC and aligned and misaligned conditions of WPT by experiment.

References

[1] S. S. Williamson, A. K. Rathore, and F. Musavi, "Industrial electronics for electric transportation: Current state-of-the-art and future challenges," *IEEE Trans. Ind. Electron.*, vol. 62, no. 5, pp. 3021–3032, May 2015.

[2] F. Wu, S. Wu, Y. Wei, P. K. Ray, and H. Liu, "Integrated wired/wireless charging system for electrical vehicles with resonant frequency tuning function," *IEEE Trans. Power Electron.*, vol. 39, no. 9, pp. 10704–10709, Sep. 2024.

[3] M. Chinthavali, O. C. Onar, S. L. Campbell, and L. M. Tolbert, "Isolated wired and wireless battery charger with integrated boost converter for PEV applications," in *Proc. IEEE Energy Convers. Congr. Expo.*, 2015, pp. 607–614.

[4] M. Elshaer, C. Bell, A. Hamid, and J. Wang, "DC–DC topology for interfacing a wireless power transfer system to an on-board conductive charger for plug-in electric vehicles," *IEEE Trans. Ind. Appl.*, vol. 57, no. 6, pp. 5552–5561, Nov./Dec. 2021.

[5] A. Ramezani and M. Narimani, "A new wireless EV charging system with integrated DC-DC magnetic element," *IEEE Trans. Transp. Electrific.*, vol. 5, no. 4, pp. 1112–1123, Dec. 2019.

[6] Y. Jia, L. Zhao, Z. Wang, C. Tang, F. Chen, and H. Feng, "Integrated LCC-LCC topology for WPT system with CC output regarding air gap and load variations," *IEEE Trans. Power Electron.*, vol. 39, no. 10, pp. 11904–11915, Oct. 2024.

[7] Y. Zhang et al., "Integration of onboard charger and wireless charging system for electric vehicles with shared coupler, compensation, and rectifier," *IEEE Trans. Ind. Electron.*, vol. 70, no. 7, pp. 7511–7514, Jul. 2023.

[8] Y. Zhang et al., "An integrated electric vehicle charging system of wireless power transfer and auxiliary power module with shared converter and magnetic coupler," *IEEE Trans. Ind. Electron.*, vol. 71, no. 9, pp. 10414–10421, Sep. 2024.

[9] Y. Wu, H. Wang, Y. Zhuang, and Y. Zhang, "A shared charging channel for power and auxiliary batteries in electric vehicles," *IEEE Trans. Ind. Electron.*, vol. 71, no. 7, pp. 8199–8203, Jul. 2024.

[10] C.-H. Jo and D.-H. Kim, "Novel compensation parameter design methodology and maximum efficiency tracking control strategy for inductive power transfer system," *IEEE Access*, vol. 10, pp. 56133–56144, 2022.

[11] H. Zhang, Y. Chen, C.-H. Jo, S.-J. Park, and D.-H. Kim, "DC-link and switched capacitor control for varying coupling conditions in inductive power transfer system for unmanned aerial vehicles," *IEEE Trans. Power Electron.*, vol. 36, no. 5, pp. 5108–5120, May 2021.

[12] Y. Chen et al., "A unipolar-duty-cycle hybrid control strategy of series–series compensated IPT system for constant-current output and efficiency optimization," *IEEE Trans. Power Electron.*, vol. 37, no. 11, pp. 13884–13901, Nov. 2022.

[13] C.-S. Wang, G. A. Covic, and O. H. Stielau, "Power transfer capability and bifurcation phenomena of loosely coupled inductive power transfer systems," *IEEE Trans. Ind. Electron.*, vol. 51, no. 1, pp. 148–157, Feb. 2004.

[14] M. Kim, D.-M. Joo, and B. K. Lee, "Design and control of inductive power transfer system for electric vehicles considering wide variation of output voltage and coupling coefficient," *IEEE Trans. Power Electron.*, vol. 34, no. 2, pp. 1197–1208, Feb. 2019.

[15] S. Ann and B. K. Lee, "Analysis of impedance tuning control and synchronous switching technique for a semibridgeless active rectifier in inductive power transfer systems for electric vehicles," *IEEE Trans. Power Electron.*, vol. 36, no. 8, pp. 8786–8798, Aug. 2021.